Materials Research. 2025; 28: e20240483
DOI: https://doi.org/10.1590/1980-5373-MR-2024-0483

Anti-Corrosion and Mechanical Performance of Graphene Oxide and Reduced Graphene Oxide Multi-Layer Coatings Applied to Nickel-Titanium Via Dip-Coating

***Pablo Forlam Ribeiro Batista*[a], *Hana Hitomi Koga*[b], *Victor Cardoso Campideli*[b], *Dalila Chaves Sicupira*[b*], *Leandro de Arruda Santos*[a]**

[a]*Universidade Federal de Minas Gerais, Escola de Engenharia, Departamento de Engenharia Metalúrgica e de Materiais, Belo Horizonte, MG, Brasil.*
[b]*Universidade Federal de Ouro Preto, Instituto de Ciências Exatas e Biológicas, Departamento de Química, Ouro Preto, MG, Brasil.*

Received: October 25, 2024; Revised: February 07, 2025; Accepted: March 16, 2025

This study investigated the mechanical and anti-corrosive properties of two graphene derivatives multi-layer coatings applied to a superelastic NiTi alloy. Several aspects of the coating process and electrochemical characterization remain unclear, including the impact of a multilayer during dip-coating on the final morphology and corrosion resistance of the system. Additionally, the relationship between long-term immersion tests, mechanical cycling and the anti-corrosion performance of these coatings requires further investigation. The coatings were formulated with GO and rGO dispersed in SEBS to be deposited as flexible nanometer films on NiTi wires using the dip-coating technique. The coating characterization was conducted through scanning electron microscopy, atomic force microscopy, X-ray diffraction and energy dispersive scattering. The mechanical performance under superelastic loading-unloading cycles was evaluated using uniaxial tensile tests. Potentiodynamic polarization and electrochemical impedance spectroscopy analyses were employed to assess corrosion. The potentiodynamic polarization results demonstrated an enhancement in corrosion resistance for the coated samples, particularly in specimens coated with rGO. Additionally, electrochemical impedance spectroscopy analysis revealed superior performance of the coating containing GO after 21 days of immersion in a simulated body fluid. These findings represent an advancement in the investigation of the NiTi surface modification by graphene derivatives.

Keywords: *Superelastic nickel-titanium, Anti-corrosion performance, Multi-layer dip-coating, Graphene-Based coating.*

1. Introduction

Since their discovery in 1963 by Buehler et al.[1], NiTi alloys have been used in a variety of applications, such as orthodontic wires, guide wires, medical stents, actuators for the aerospace industry, devices based on the high damping capacity of shape memory alloys, and others[2]. NiTi is the material of choice to produce modern endodontic rotary instruments and is preferred for specific applications over conventional implant materials due to their high biocompatibility and distinct properties[3], such as superelasticity (SE) and shape memory effect (SME). SE occurs by the stress-induced martensitic transformation upon loading, and the subsequent reverse transformation upon unloading, allowing the recovery of large deformations. The SME is the recovery of an apparent plastic deformation through structural transformation when the alloy is heated above a certain limit[4].

Although a high corrosion resistance is expected due to the spontaneous formation of a thin passive film of TiO_2 on the surface of near-equiatomicNiTi alloys, its stability against corrosion strongly depends on the surface conditions[5]. Several surface modification techniques have been investigated to improve the surface of NiTi alloys, such as electrochemical processes and dip-coating[6-9]. Comparing coating techniques, multilayer dip coating is simple, inexpensive, and ideal for uniform, multilayer films, but can be time-consuming for thick films. Electrochemical deposition offers precision and strong adhesion, but is limited to conductive substrates. Spray coating is fast and flexible for large areas, but less precise for complex geometries[10,11].

Dip-coating is applicable to many materials beyond NiTi alloys, including stainless steel for biomedical and industrial uses, aluminum and titanium alloys for aerospace and automotive, ceramics for protective films, and polymers for functional coatings in electronics and textiles. However, challenges like material wastage, thickness uniformity on complex geometries, and adhesion issues can arise. Despite these limitations, advances in surface preparation and automation continue to enhance its utility, making it a valuable method for scalable applications across industries[12].

Aun et al.[13]observed that a TiO_2nanometric coat may be successful in preventing premature failure and corrosion of

*e-mail: dalila@ufop.edu.br

NiTi endodontic instruments. Guo et al.[14] used selective laser melting to coat a NiTi alloy with graphene oxide aiming to increase its corrosion resistance.

Graphene, an atomically thin layer of carbon, has several unique physical and chemical characteristics[15,16]. This nanometric two-dimensional honeycomb structure has attracted great attention in various fields[17] due to its high impermeability and hydrophobicity[17]. Furthermore, graphene can offer excellent wear resistance, unlike conventional materials, due to its high hardness, low friction coefficient, and lubrication properties[18]. Its most relevant characteristics commonly qualify graphene as an ideal material for anti-corrosive coatings[19]. Therefore, it can be considered a potential candidate for improving the corrosion and wear resistance of metallic materials.

Graphene oxide (GO) and reduced graphene oxide (rGO) coatings are particularly valued for their mechanical strength, flexibility, and electrical conductivity. However, challenges such as controlling the reduction level of GO to achieve desired rGO properties and ensuring uniform coating application persists. Additionally, while rGO's hydrophobicity enhances corrosion resistance, it can also hinder adhesion to certain substrates, necessitating surface modifications or the use of adhesion promoters. When compared to other advanced coatings, such as transition metal dichalcogenides (TMDs) and metal-organic frameworks (MOFs), GO and rGO offer distinct advantages. TMDs, like MoS_2, provide excellent lubrication properties but may suffer from oxidation under certain conditions. MOFs are known for their high porosity and tunable structures, yet their stability, especially in humid environments, can be a concern[20-23].

The affinity of dip-coated GO and rGO solutions to NiTi substrates is explained by chemical and physical interactions. The mechanism is described as follows: Pre-treatment (e.g., acid etching) of the substrate cleans and activates the surface, increasing its energy and enhancing wettability. GO's oxygen-rich functional groups (hydroxyl, carboxyl, and epoxy) form strong hydrogen bonds and electrostatic interactions with the substrate, promoting adhesion. In rGO, the reduction of oxygen groups leads to a decrease in chemical affinity, but it enhances hydrophobic interactions, resulting in a more compact layer. During the dip-coating process, the solution spreads due to capillary action, and a liquid film remains after withdrawal. The thickness of this layer is governed by solution viscosity and withdrawal speed. The solvent evaporates, solidifying the layer, and multilayer coatings build uniformity and strength with repeated dips. This mechanism ensures good adhesion and uniform deposition, which are essential for improving NiTi's surface[24-27].

Recently, Araujo et al.[6]developed coatings based on graphene oxide (GO) and reduced graphene oxide (rGO) incorporated into a block copolymer of styrene–ethylene–butylene–styrene (SEBS) to be applied to the NiTi surface via the dip-coating technique with promising results in terms of corrosion resistance. Nevertheless, several aspects of the coating process and electrochemical characterization remain unclear, including the impact of a multilayer sequence during dip-coating on the final morphology and corrosion resistance of the system. Additionally, the relationship between long-term immersion tests, mechanical cycling, and the anti-corrosion performance of these coatings requires further investigation.

Thus, in this work, we delve deeper into the methodology proposed by Araujo et al.[6] to explore different aspects involved in the dip-coating process and corrosion behavior of a NiTi alloy coated with graphene derivatives after immersion test in SBF solution and mechanical cycles. Multi-layer coatings were applied to the NiTi samples by the dip-coating technique, being these coatings consisted of a dispersion of SEBS doped with GO or rGO. The preference for employing SEBS stems from its extensively documented biocompatible qualities[28,29]. GO and rGOcoatings have been investigated for their potential to enhance the thermal stability of NiTi alloys, particularly in applications subject to fluctuating temperatures. While GO and rGO coatings have demonstrated potential in enhancing the thermal stability and corrosion resistance of NiTi alloys, their effectiveness under fluctuating temperatures may vary based on specific material properties and environmental conditions[30,31]. The thermal stability of coatings was assessed in terms of their ability to maintain mechanical integrity and anti-corrosive properties under fluctuating temperature conditions. The electrochemical tests were carried out at intervals of 0 to 21 days in simulated body fluid (SBF) solution with temperature and pH conditions similar to the human body. To discern the efficacy and endurance of these applied coatings after superelastic strain cycles, uniaxial loading sequences and scanning electron microscopy (SEM) investigations were enlisted.

2. Experimental Procedure

SuperelasticNiTi wires with a nominal composition of 50.8 at% Ni (supplied by NDC, Fremont, CA, USA) were used. These wires had a 1 mm diameter and were cut into 12 cm long specimens. Before the coating process, the samples were etched in a solution of phosphoric acid, oxygen peroxide, and distilled water in the proportion 5:3:2 at 80 ºC for 20 min[13,32] to remove the oxides and manufacturing defects from the surface.

Two nanofillers were applied by dip-coating as follows: 1) 30 mg of GO dispersed in the SEBS matrix, and 2) 30 mg of rGO dispersed in SEBS. Before the addition of GO or rGO, 3.0 g of the SEBS copolymer was dissolved into 25.0 mL toluene under constant agitation in an ultrasonic bath at 50 ºC for 30 min. Then, GO or rGO was incorporated and dispersed in an ultrasonic bath for another 30 min, at room temperature, to achieve a stable and homogeneous dispersion. Two-thirds of the sample's length was dipped into the solutions with the help of a dip coater apparatus (TMAX, equipped with a WHL-30BL oven). The immersion and withdrawing speeds were approximately 10 cm/min. The immersion process was carried out for 1 minute, and then the samples were dried for 3 minutes at room temperature for complete evaporation of the solvents. This dip-coating procedure was repeated five times for each sample, resulting in five layer coated samples.

The morphology of the surfaces was analyzed employing field emission-SEM (FEI Quanta 3D) using an acceleration potential of 15 kV and secondary electron imaging. Qualitative composition data was obtained through energy dispersive spectroscopy (EDS). To evaluate the average roughness (Ra) of the coatings, atomic force microscopy (AFM) measurements

were acquired on a 30 × 30 μm^2 area using a Cypher ES microscope (Asylum Research) in the tapping mode with a cantilever force of 0.2 N/m and a resonant frequency of 23 kHz.

The mechanical performance of the coatings was evaluated through uniaxial tensile tests using a universal test machine (Instron 5582), following the ASTM F2516-18 standard, with a strain rate of 0.016 s^{-1} (strain per second)[33]. The samples were subjected to 10 superelastic cycles, being loaded until ε= 6% and then unloaded until the complete load removal. SEM was used to characterize possible damage in the coatings caused by these efforts. Figure 1 shows a superelastic uniaxial tensile cycle like the ones performed in this work. During the loading of a superelastic alloy, it is observed the regular elastic strain of the sample until critical stress (point 2 in Figure 1), then the start of the transformation from austenite to martensite takes place, resulting in the stress plateau until point 3. From point 3, the induced martensite begins to deform elastically until point 4 is reached, which also delimits the maximum load that the alloy can withstand without any permanent (plastic) deformation. After removing the load (points 5 to 6), the process of returning to the stable austenitic state takes place, resulting in the total recovery of the deformation at point 7[4,34].

To verify the anti-corrosion performance of the graphene-based coatings and simulate real-world conditions while predicting the material's durability over time, both coated and uncoated samples were subjected to an immersion test with intervals ranging from 0 to 21 days.All prepared specimens were kept at 37 °C in containers with 10 to 20 mL of a solution that simulates body fluid (SBF) with its composition described in Table 1. Electrochemical tests were performed using an AUTOLAB PGSTAT302N potentiostat and a three-electrode flat cell consisting of a working electrode, an Ag/AgCl reference electrode, and a platinum electrode as the counter. The coated sample was immersed in a glass cell containing about 150 mL of SBF solutionwith pH = 7.4 at 37 ± 2°C (human body temperature). Potentiodynamic (PP) polarization tests were performed after 1 h of open circuit potential (OCP) stabilization at a constant sweep rate of 0.167 mV/s from − 250 mV_{ocp} to + 250 mV_{ocp}. Corrosion current density (I_{corr}) and corrosion potential (E_{corr}) were determined by the Tafel extrapolation method. Electrochemical Impedance Spectroscopy (EIS) test was performed at OCP, in the frequency range 100kHz− 10 mHz with a disturbance potential of 10 mV and 10 points per decade. PP and EIS techniques were performed for coated samples before and after tensile tests.

3. Results and Discussion

The EDS analysis confirmed an elevated presence of carbon (Figure 2) for the two coatings in comparison with the bare substrate. For the sample coated with GO (Figure 2), an area with a flowed adhesion of the coating was selected. The elemental map makes it clear that the coating is practically composed of carbon. In the exposed area, we can see red spots corresponding to nickel. Generally, it is not easy to detect nickel on the NiTi alloy elemental maps due to the formation of TiO_2 on the surface of the sample[35].

The morphology of the studied surfaces obtained by SEM is shown in Figure 3. When comparing the two studied coatings, the images suggest that rGO+SEBS forms an even and uniform layer, while GO+SEBS presents a rougher aspect in the analyzed area. From AFM analyses (Figure 4), it can be observed that the surface roughness measured after the coatings was significantly different from the one measured for the bare substrate (22.65 nm): GO+SEBS presented a roughness of 1.10 nm, while rGO+SEBS depicted 1.20 nm.

Table 1. Reagents needed to prepare 1000 mL of SBF solution.

Reagents	Amount	Molecular mass (u)
NaCl	8.036 g	58.4
$NaHCO_3$	0.352 g	84.01
KCl	0.225 g	74.56
$K_2HPO_4.3H_2O$	0.230 g	228.23
$MgCl_2.6H_2O$	0.311 g	203.30
1M HCl	40 mL	...
$CaCl_2$	0.293 g	110.98
Na_2SO_4	0.072 g	142.04
tris(hydroxymethyl)aminomethane*	6.063 g	121.14

* $H_2NC(CH_2OH)_3$

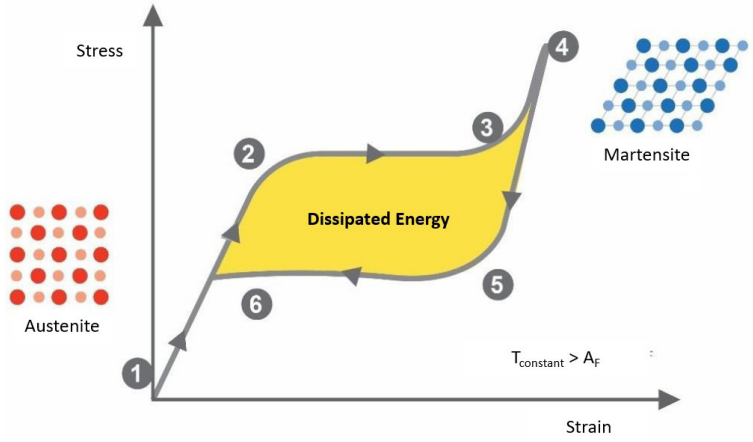

Figure 1. Typical stress-strain curve for a superelastic uniaxial tensile cycle.

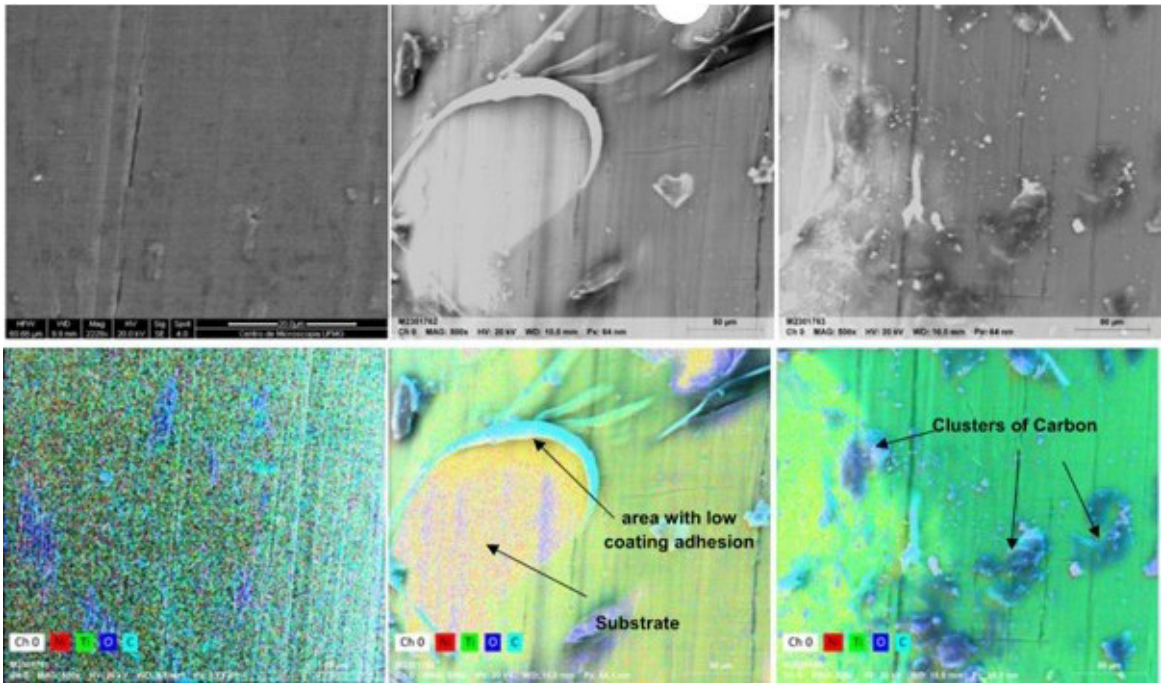

Figure 2. SEM images and respective elemental maps (colored images) obtained through EDS analysis for bare NiTisubtrate (left), NiTi coated with GO (middle) and NiTi coated with rGO (right).

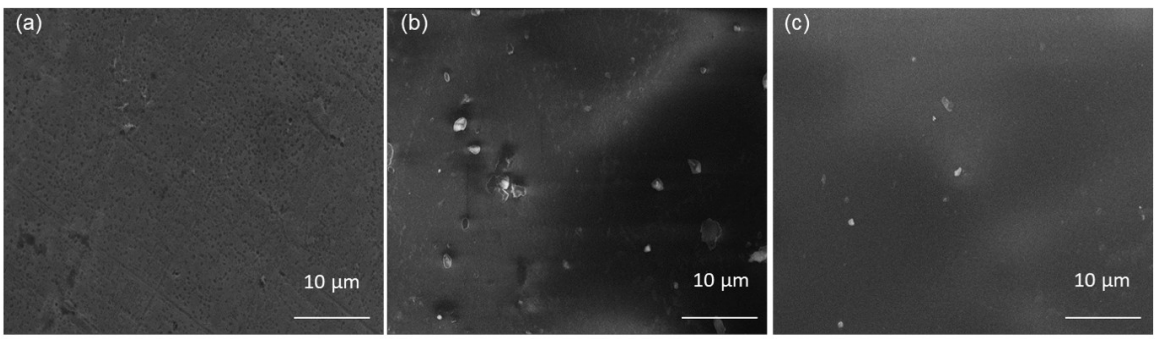

Figure 3. SEM images of (a) Bare NiTi substrate, (b) NiTi coated with GO, (c) and NiTi coated with rGO amplified 8000x.

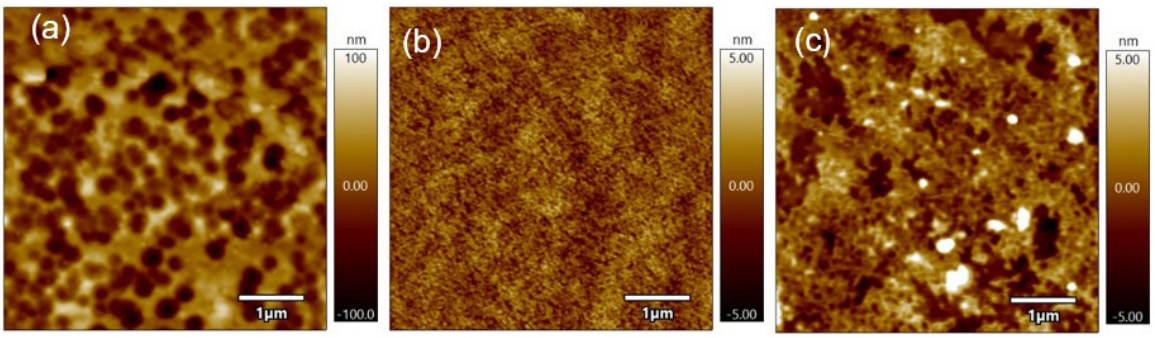

Figure 4. AFM images for the samples: (a) bare NiTi substrate, (b) NiTi coated with GO, and (c) NiTi coated with rGO.

Figure 5 shows the morphology of the coatings after tensile test up to $\varepsilon = 6\%$, after 10 loading cycles. Comparing with Figure 3, we conclude that no relevant morphological damages were caused during this mechanical work. This result is consistent with the one published by Araujo et al.[6], reinforcing the relevance of NiTi alloys being coated with materials that may undergo large deformation cycles.

Potentiodynamic polarization (PP), when applied to samples of NiTi alloys, is used to obtain a current signal that relates potential and current during the electrochemical

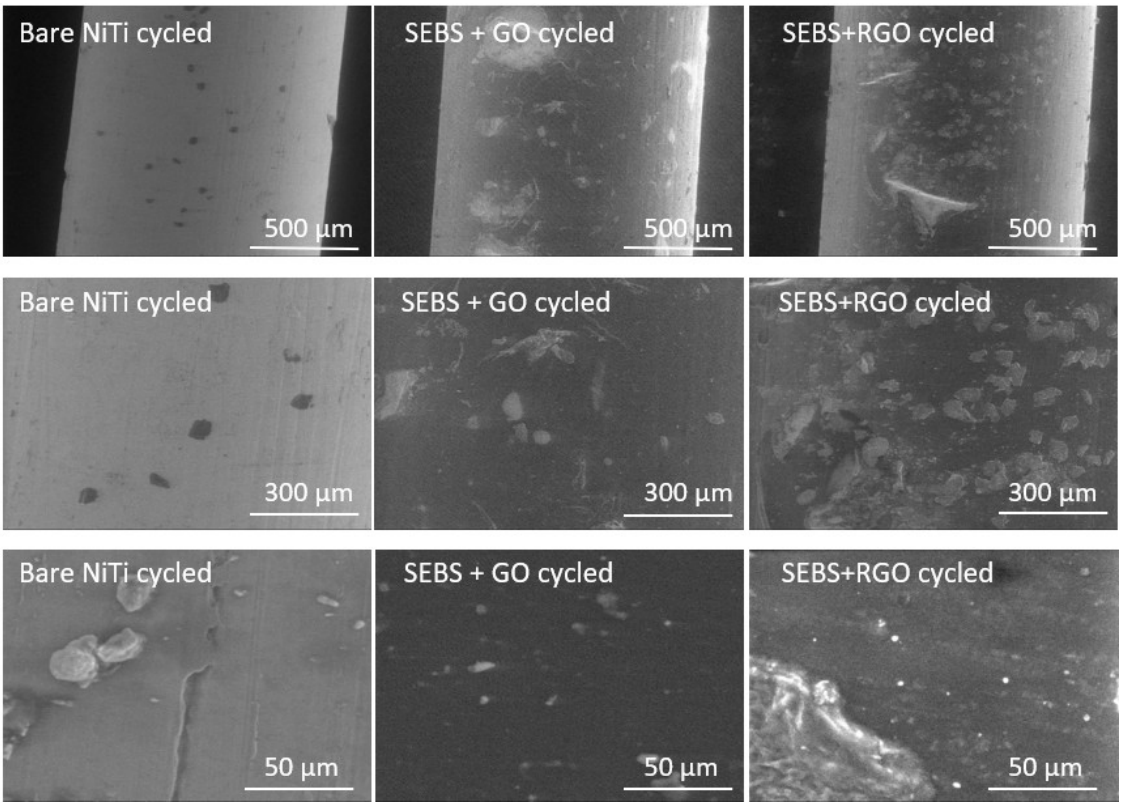

Figure 5. SEM images of the samples after the superelastic uniaxial tensile cycles. The amplification was 100x in the upper row, 250x in the middle row and 8000x in the lower row.

polarization process. Analysis of PP in metal coatings reflects the barrier and strength effects of the coatings, being useful to reveal the protective nature of the coating together with the protective barrier provided by the titanium oxide formed on the surface of the substrate[6]. The PP curves performed in SBF solution for NiTi samples coated with GO+SEBS, rGO+SEBS, and bare NiTi before and after the tensile tests are shown in Figure 6. The parameters obtained applying the Tafel extrapolation method are in Table 2. The corrosion potential (E_{corr}) shows susceptibility to corrosion, the more negative it is, the more active the surface, making it more likely to present corrosion[14]. I_{corr} allows analyzing the corrosion rate, the lower the corrosion rate, the greater the corrosion resistance[24]. As shown in Table 2, there is a difference in the corrosion potential of the samples, the E_{corr} for the samples coated with GO (−0.06 V) and rGO (−0.20 V) before the tensile test is less negative than the sample without coating (−0.33 V). The I_{corr} for coated samples is an order of magnitude greater than the uncoated sample, demonstrating that although the coating has a protective characteristic, preventing the corrosion process of the NiTi alloy, the process occurs more rapidly with the coating. This means that the two coated samples have higher corrosion protection and an improvement in protection compared to the bare NiTi sample. The results suggest a better corrosion resistance for the rGO sample, which can be explained by its hydrophobic and waterproofing properties[36]. Compared to the previous work[6], although the obtained Ecorr values are similar, the Icorr values in this study are approximately 1000 times smaller.

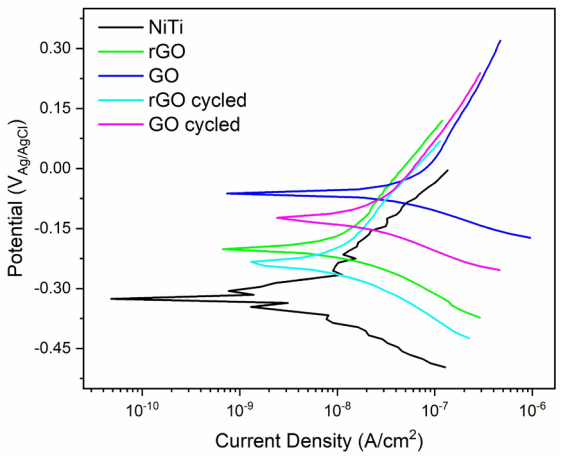

Figure 6. Potentiodynamic polarization curves of bare NiTi and samples coated with GO and rGO before and after cycling.

Table 2. Electrochemical parameters obtained by Tafel extrapolation of potentiodynamic polarization.

Sample	Ecorr (V)	icorr (A/cm^2)
NiTi	-0.33	3.34 x 10^{-9}
rGO	-0.20	2.20 x 10^{-8}
GO	-0.06	6.01 x 10^{-8}
rGO cycled	-0.24	3.53 x 10^{-9}
GO cycled	-0.13	3.32 x 10^{-8}

After the tensile tests, the GO (−0.13 V) and rGO (−0.24 V) coatings still showed a higher corrosion potential than the uncoated sample (−0.33V). Therefore, even after the mechanical work, the coatings still provide significant protection against corrosion. Comparing the GO and rGO samples before and after the tensile tests, we observed a small decrease in the corrosion potential in more negative directions and the corrosion current remained in the same order of magnitude for the GO sample and showed an order of magnitude lower for the rGO sample compared to NiTi. Thus, from a corrosion point of view, there was no deterioration of the coating with the cycling.

SEM images of the tested surface after etching are shown in Figure 7. The uncoated NiTi surface has etch marks across its surface. Analyzing both GO and rGO samples revealed areas with increased corrosion degradation, indicating a heterogeneous corrosion process[6]. In the qualitative analysis, a large number of corroded areas were observed in the GO sample compared to the rGO sample, indicating that the samples coated with rGO have a greater ability to protect the surface. The SEM observations support the results obtained by PP analysis.

Analyzing the Nyquist diagram in Figure 8b and 8c, the arc impedance of the coated samples after the periods in immersion shows an increase in its diameter, suggesting an increase in the coating corrosion properties over immersion time. On the other hand, the arc impedance for uncoated NiTi (Figure 8a) remained relatively constant, showing no effect on its corrosion protection property. The rGO sample showed better corrosion resistance and a lower corrosion rate than the GO one in the beginning. However, under the effect of the immersion test in a corrosive environment, the

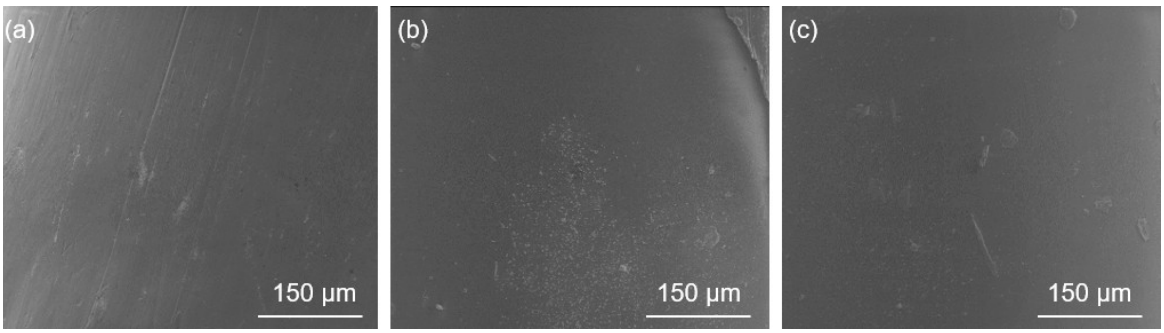

Figure 7. SEM surface images of the (a) bare NiTi sample, (b) GO coated sample, and (c) rGO coated sample after corrosion tests.

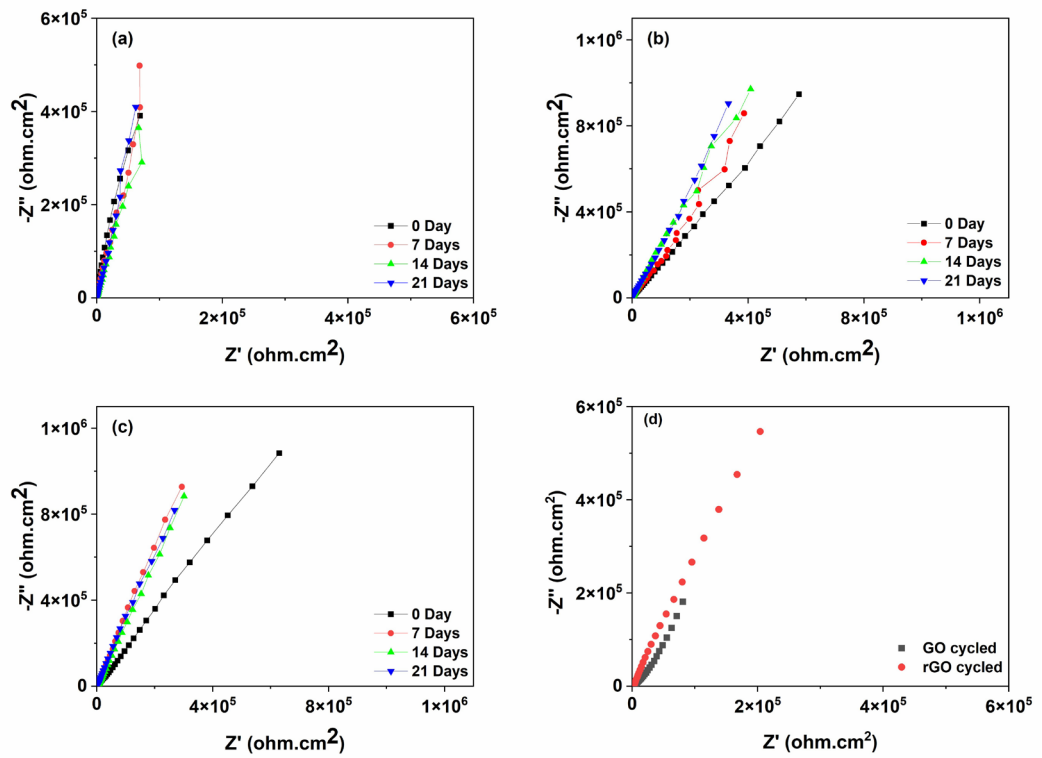

Figure 8. Nyquist diagrams of samples in SBF solution: (a) bare NiTi, (b) sample with GO, (c) sample with rGO, and (d) samples GO and rGO coated after cycling.

GO sample showed a lower degradation of its protection properties against corrosion. The cycled GO and rGO samples (Figure 8d) have a smaller diameter of semicircle compared to not cycled samples, demonstrating a loss of corrosion resistance after cycling. However, the decrease in the diameter of the impedance arc for the rGO sample is smaller than that for the GO sample, suggesting that there is less degradation of the coating with rGO.

The results obtained from electrochemical impedance spectroscopy (EIS) can be represented by the equivalent circuit model for both the uncoated NiTi alloy (Figure 9a) and for the coated samples before and after cycling (Figure 9b). The model represents the resistance of the electrolyte solution (Rs), the capacitance of the electrolyte/coating interface (Cc), the resistance of the electrolyte/coating interface (Rc), the double layer capacitance (Cdl), and the charge transfer resistance of the corrosion reaction (Rct). The parameters obtained in the equivalent circuit are presented in Table 3. Polarization resistance (Rp) is the effective resistance of the circuit (Table 3) and can be calculated by Equation 1 for coated samples and Equation 2 for the uncoated sample[34]

$$Rp = Rc + Rct \quad (1)$$

$$Rp = Rc \quad (2)$$

In Figure 10, it is possible to observe that both GO and rGO have a higher polarization resistance value compared to the pure NiTi sample, suggesting that the coated samples have greater corrosion resistance than the NiTi sample. The coated samples showed an increase in corrosion resistance over the days, with this increase being greater for the rGO than for the GO coating after 21 days of immersion. Despite this, the variation in corrosion resistance for both samples over the days is small, which suggests that the coatings are effective as a protective barrier against corrosion in SBF solution. The degradation of rGO coatings reduces their protective performance, exposes the substrate to corrosion, and weakens mechanical integrity. It may also lead to cytotoxicity due to leaching particles, limiting rGO's suitability for long-term or high-stress applications. To mitigate degradation, strategies include functionalizing rGO with silanes or polymers to improve stability[17], incorporating rGO into hybrid coatings with materials like TiO_2[27], and optimizing dip-coating parameters for uniformity and adhesion[37]. Adding protective barrier layers, such as polymeric films, can further shield rGO from corrosive environments[38].

To understand the performance of the coating after the tensile test, an EIS test was also performed on the SBF solution after the coated samples were subjected to the tensile tests. Figure 11 shows Rp values for the coated samples before and after the tensile test. Both samples showed a decrease in corrosion resistance. Although the resistance of the rGO sample decreases, it remains greater than that of the GO-coated sample, suggesting smaller deterioration upon cycling.

Figure 12 shows the effect of immersion in SBF for NiTi samples. Using the SEM, it is possible to observe that after 21 days of immersion, the uncoated NiTi sample shows corrosion spots. On the other hand, the GO and rGO samples show dissolution of the coating in several regions. The rGO sample presents a higher density of defective regions in the coating caused by immersion corrosion in the SBF solution. Table 4 summarizes the corrosion and mechanical performance of GO and rGO coatings compared to uncoated NiTi samples.

The corrosion mechanism is explained by equations (3) to (8). There is an oxidation process of NiTiand also reduction processes with electrons released during oxidation[30]. The reduction of O_2 occurs and the reactions that take place at the cathode are:

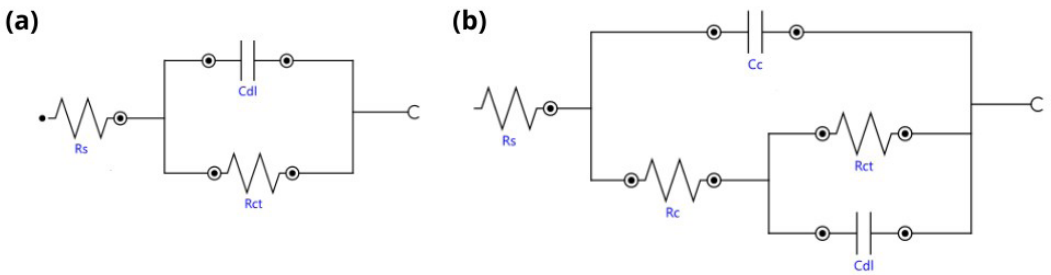

Figure 9. Equivalent circuit for samples without coatings (a) and (b) for coated samples before and after cycling.

Table 3. Fitting parameters for experimental EIS data.

	Rc (MΩ.cm^2)			Rct (MΩ.cm^2)			Rp (MΩ.cm^2)		
Sample	NiTi	GO	rGO	NiTi	GO	rGO	NiTi	GO	rGO
0days	-	4.9	5.2	20.8	25.6	27.9	20.8	30.6	33.1
7days	-	3.7	6.2	18.6	31.4	43.8	18.6	35.2	50.1
14days	-	6.7	5.7	15.3	38.2	41.5	15.3	44.9	47.3
21days	-	5.5	6.2	22.9	44.1	36.8	22.9	49.6	42.9
After cycling	-	0.6	3.7	-	6.9	22.1	-	7.5	25.8

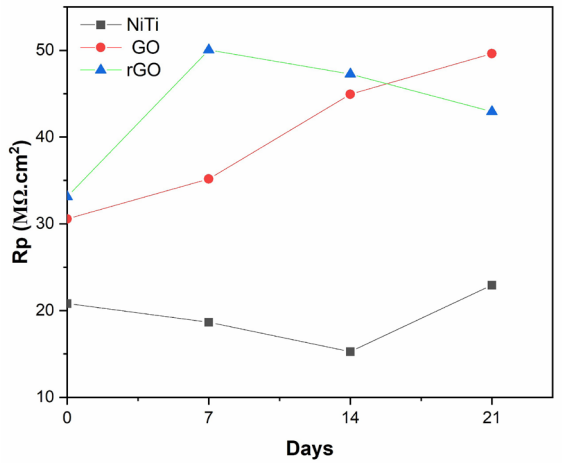

Figure 10. Rp values for samples over the immersion days in SBF solution.

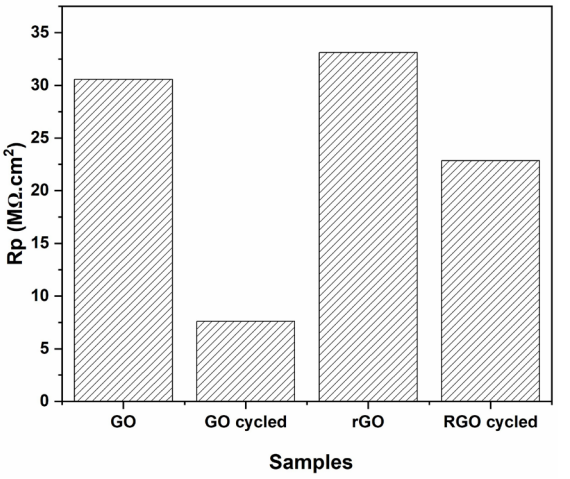

Figure 11. Rp values for coated samples before and after cycling.

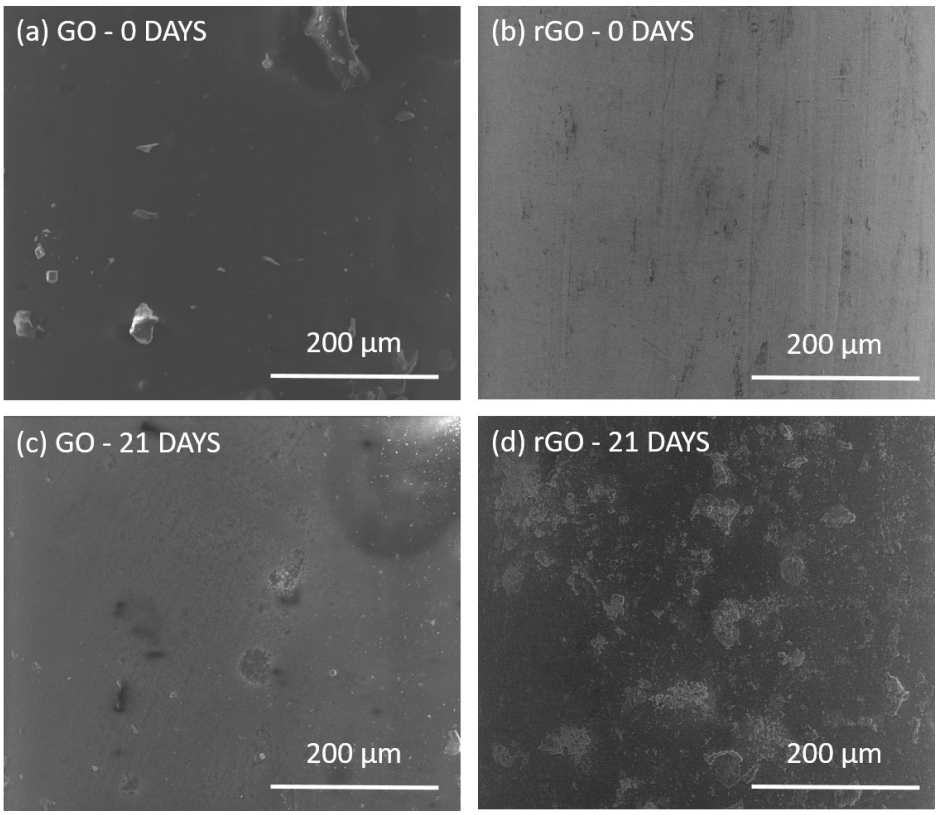

Figure 12. SEM surface images of samples before immersion in SBF solution: (a) coated with GO, and (b) coated with rGO. After 21 days of immersion: (c) coated with GO and (d) coated with rGO.

$$O_2(g) + 2H_2O + 2e^- \rightarrow 2OH + 2OH^-_{(aq)} \quad (3)$$

$$OH_{(aq)} + e^- \rightarrow OH^-_{(aq)} \quad (4)$$

Corrosion products form on the anode:

$$3Ni + 6OH^- \rightarrow 3Ni(OH)_2 + 6e^- \quad (5)$$

$$Ni(OH)_2 \rightarrow NiO.H_2O \quad (6)$$

$$Ti + 4OH^- \rightarrow TiH_4O_4 + 4e^- \quad (7)$$

$$TiH_4O_4 \rightarrow TiO_2.2H_2O \quad (8)$$

Table 4. Summary of the corrosion and mechanical performance of GO and rGO coatings compared to uncoated NiTi samples.

Parameter	GO Coating	rGO Coating	Baseline NiTi
Corrosion Potential (Ecorr)	Higher than baseline (-0.06 V before cycling)	Higher than baseline (-0.20 V before cycling)	More negative (-0.33 V)
Corrosion Current Density (Icorr)	Low current; indicating high corrosion resistance	Low current; indicating high corrosion resistance	Low current; indicating high corrosion resistance
Long-term Stability (Immersion)	Increased corrosion resistance over 21 days in SBF	Increased corrosion resistance over 21 days in SBF	Stable over 21 days in SBF
Performance After Cycling	Susceptible to increased corrosion rate after cycling	Susceptible to increased corrosion rate after cycling	-
Surface Integrity for cycled samples (SEM)	No significant damage during superelastic cycles	No significant damage during superelastic cycles	Visible surface wear during stress cycles
Roughness (Ra)	~1.10 nm (reduced from baseline 22.65 nm)	~1.20 nm (reduced from baseline 22.65 nm)	~22.65 nm (higher surface roughness)

NiTi coated with GO or rGO presents a layer that prevents the metal surface from its contact with the OH^- ion, in addition to restricting anodic oxidation and inhibiting the reactions of the corrosion process of the NiTi alloy[30].

Xue et al.[39] studied the delay of the O_2 reduction reaction, which occurs due to the decrease of the active surface available to be attacked in a corrosive environment due to the use of a GO coating. In addition, the authors reported a decrease in the resistance of the active surface due to the slight electrical conductivity of GO. The results obtained in the present work are consistent with studies carried out by other authors[30,39,40]. The rGO coating has a smaller number of functional groups containing oxygen, resulting in a coating with hydrophobic properties and waterproofing. The reduction of H_2O, O_2, and Cl^- at the NiTi alloy/coating interface improves the corrosion resistance of the rGO coating. Thus, the corrosion resistance exhibited by the rGO coating may be attributed to its hydrophobic properties[36].

The rGO exhibits enhanced corrosion resistance compared to GO primarily due to its increased hydrophobicity and decreased oxygen-containing functional groups. The reduction process of GO to rGO removes a significant number of oxygen functionalities, resulting in a more hydrophobic surface. This hydrophobicity minimizes water adsorption on the material's surface, thereby reducing the electrochemical reactions that lead to corrosion. Additionally, the fewer oxygen groups in rGO decrease the number of active sites susceptible to oxidative reactions, further enhancing its corrosion resistance. These combined factors make rGO a more effective barrier against corrosive environments compared to GO[41,42]. This is consistent with the potentiodynamic polarization depicted in this work. However, the results related to the long-term capacity of these coatings suggest that GO is the most resistant to corrosion over the days. It can be explained by the behavior exhibited by this coating on prolonged exposure to this specific corrosion medium. Although the rGO coatings provide better instant protection due to their hydrophobic property, the GO coating can passivate the metallic substrate, improving protection against the corrosive environment with time[43]. This is reinforced by the SEM images after 21 days of immersion shown in Figure 12. Furthermore, several studies report that rGO coatings tend to present better anticorrosive properties. Those studies focus on electrochemical analyses in solutions containing NaCl[30,36,39,41] or in solutions with different compositions[6]. Only a few studies used SBF or Hank's solution as a corrosion medium and they do not evaluate the anti-corrosion performance for a long period. Thus, the long-term behavior of the rGO coating in SBF solution, presenting a lower performance compared with GO, may also be associated with its behavior in solutions that simulate human body fluid, which is a more complex medium.

4. Conclusions

Based on the results depicted in this study, the following conclusions were drawn:

- Both NiTi samples coated with GO and rGO showed roughness close to 1 nm, much lower in comparison with the uncoated sample (close to 22 nm).
- The coatings containing GO and rGO were able to maintain their integrity during superelastic loading cycles. No significant morphological damage was observed after mechanical work.
- Potentiodynamic polarization analysis showed that both coated samples have their anti-corrosion capacity increased when compared with the bare-NiTi sample, with the rGO coating being the most efficient one.
- The EIS analysis showed that the corrosion performance of the rGO coating presents a more pronounced decrease in comparison with the GO coating throughout the 21-day immersion test. Despite this, the variation in corrosion resistance for both samples over the days is small, which suggests that the coatings are effective as a protective barrier against corrosion in SBF solution.
- On the other hand, the anticorrosive capacity of the GO coating showed a more significant deterioration after the applied mechanical cycles compared with rGO coating.
- The coatings demonstrated resilience to mechanical stresses, which are often exacerbated by thermal fluctuations. Furthermore, these coatings exhibited capacity to withstand prolonged exposure to corrosive environments, which are characteristic of fluctuating thermal conditions. Graphene-based materials are recognized for their exceptional thermal conductivity and stability, which can facilitate heat dissipation and mitigate thermal stresses on the NiTi substrate, thereby enhancing durability in environments with temperature variations. This

combination of mechanical and electrochemical performance metrics supports the suitability of these coatings for applications that involve the presence of thermal and mechanical stresses, such as in biomedical devices or aerospace components.

Subsequent studies on graphene-based coatings could entail the optimization of coating thickness through the modulation of dip-coating parameters, with the objective of enhancing corrosion resistance and mechanical performance. Exploration of hybrid coatings comprising nanomaterials, such as TiO_2 or carbon nanotubes (CNTs), has the potential to introduce multifunctional properties, including enhanced thermal stability or wear resistance. Long-term environmental exposure studies, incorporating cyclic thermal and mechanical stresses, are essential for validating durability in real-world conditions. The functionalization of GO/rGO with silanes or peptides could enhance adhesion, hydrophobicity, and biocompatibility. Dynamic corrosion and wear studies, such as tribocorrosion testing, provide insights into performance under combined stresses. Application-specific testing, such as the use of simulated body fluid for implants or thermal cycling for aerospace components, can optimize coatings for specialized uses. These investigations will advance the scalability and applicability of graphene-based coatings for diverse industries.

5. Acknowledgments

The authors would like to thank the Microscopy Center at UFMG and the Carbon Nanostructures Chemistry Laboratory at CDTN. Also acknowledge the support of FAPEMIG, CNPq, Capes, and PRPq/UFMG and PROPPI/UFOP.

6. References

1. Buehler WJ, Gilfrich JV, Wiley RC. Effect of low-temperature phase changes on the mechanical properties of alloys near composition TiNi. J Appl Phys. 1963;34(5)
2. Van Humbeeck J. Non-medical applications of shape memory alloys. Mater Sci Eng A. 1999;273–275:134-48.
3. Peters OA. Current challenges and concepts in the preparation of root canal systems: a review. J Endod. 2004;30(8):559-67.
4. Otsuka K, Ren X. Physical metallurgy of Ti–Ni-based shape memory alloys. Prog Mater Sci. 2005;50(5):511-678.
5. Milošev I, Kapun B. The corrosion resistance of Nitinol alloy in simulated physiological solutions Part 2: the effect of surface treatment. Mater Sci Eng C. 2012;32(5):1068-77.
6. Araujo AF, Ferreira MVF, Felisberto MDV, Sicupira DC, Santos LA. Corrosion resistance of a superelasticNiTi alloy coated with graphene–based coatings. Prog Org Coat. 2022;165:106727.
7. Lopes NIA, Freire NHJ, Resende PD, Silva JD, Santos LA, Béclin F, et al. ToF-SIMS characterization of nanostructured ZrO2 coatings applied to near equiatomic Ni-Ti alloy. Mater Res. 2019;22(1):e20190189. https://doi.org/10.1590/1980-5373-MR-2019-0189
8. Lopes NIA, Henrique Jardim Freire N, Resende PD, Santos LA, Buono VTL. Electrochemical deposition and characterization of ZrO2 ceramic nanocoatings on superelasticNiTi alloy. Appl Surf Sci. 2018;450:21-30.
9. Safavi MS, Bordbar-Khiabani A, Walsh FC, Mozafari M, Khalil-Allafi J. Surface modified NiTi smart biomaterials: surface engineering and biological compatibility. Curr Opin Biomed Eng. 2023;25:100429.
10. Hossain MI, Mansour S. A critical overview of thin films coating technologies for energy applications. Cogent Eng. 2023;10(1):2179467.
11. Tonelli D, Scavetta E, Gualandi I. Electrochemical deposition of nanomaterials for electrochemical sensing. Sensors (Basel). 2019;19(5):1186.
12. Remanan S, Pulikkalparambil H, Rangappa SM, Siengchin S, Parameswaranpillai J, Das NC. Hydrophobic and hydrophilic polymer coatings. In: Rangappa SM, Parameswaranpillai J, Siengchin S, editors. Polymer coatings. Boca Raton: CRC Press; 2020. p. 247-68.
13. Aun DP, Peixoto IFDC, Houmard M, Buono VTL. Enhancement of NiTisuperelastic endodontic instruments by TiO2 coating. Mater Sci Eng C. 2016;68:675-80.
14. Guo Y, Xu Z, Wang Q, Zu S, Liu M, Yu Z, et al. Corrosion resistance and biocompatibility of graphene oxide coating on the surface of the additively manufactured NiTi alloy. Prog Org Coat. 2022;164:106722.
15. Sahu SC, Samantara AK, Seth M, Parwaiz S, Singh BP, Rath PC, et al. A facile electrochemical approach for development of highly corrosion protective coatings using graphene nanosheets. Electrochem Commun. 2013;32:22-6.
16. Krishnan MA, Aneja KS, Shaikh A, Bohm S, Sarkar K, Bohm HLM, et al. Graphene-based anticorrosive coatings for copper. RSC Advances. 2018;8(1):499-507.
17. Sun P, Wang K, Zhu H. Recent developments in graphene-based membranes: structure, mass-transport mechanism and potential applications. Adv Mater. 2016;28(12):2287-310. http://doi.org/10.1002/adma.201502595.
18. Peng Y, Wang Z, Zou K. Friction and wear properties of different types of graphene nanosheets as effective solid lubricants. Langmuir. 2015;31(28):7782-91.
19. Yu F, Camilli L, Wang T, Mackenzie DMA, Curioni M, Akid R, et al. Complete long-term corrosion protection with chemical vapor deposited graphene. Carbon. 2018;132:78-84.
20. Xavier JR, Ramesh B. Experimental investigation of polymer matrix filled with silanized cerium carbide nanofillers and graphene oxide in automotive components. Appl Nanoscience. 2023;13(9):6133-49.
21. Raj Xavier J, Ramesh B. A study on the effect of multifunctional tantalum carbide nanofillers incorporated graphene oxide structure in the epoxy resin for the applications in the shipbuilding industry. Mater Sci Eng B. 2023;289:116234.
22. Vinodhini SP, Xavier JR. Investigation of anticorrosion and mechanical properties of azole functionalized graphene oxide encapsulated epoxy coatings on mild steel. J Fail Anal Prev. 2021;21(2):649-61.
23. Beryl JR, Xavier JR. Investigation of smart graphene oxide multilayer nanocoating for improved steel structural protection in natural seawater. J Mater Sci. 2024;59(2):458-90.
24. Panja K, Vivek N, Ramar K. Surface coating of nickel-titanium (Ni-Ti) pediatric rotary file using graphene oxide: a scanning electron microscopy analysis. Cureus. 2024;16(8):e66632.
25. Frederichi D, Scaliante MHNO, Bergamasco R. Structured photocatalytic systems: photocatalytic coatings on low-cost structures for treatment of water contaminated with micropollutants—a short review. Environ Sci Pollut Res Int. 2021;28(19):23610-33. http://doi.org/10.1007/s11356-020-10022-9.
26. Liu Y, Fei B, Xin JH. Functionalization of fabrics with Graphene-based coatings: mechanisms, approaches, and functions. Coatings. 2023;13(9):1580.
27. Shanmugapriya SV, Padma RA, Senthil KP, Selvamani ST, Mandal TK. Sol–gel derived Al2O3/Gr/HAP nanocomposite coatings on Ti–6Al–4V alloy for enhancing tribo-mech properties and antibacterial activity for bone implants. Appl Phys, A Mater Sci Process. 2022;128(8):635.

28. Gennari CGM, Quaroni GMG, Creton C, Minghetti P, Cilurzo F. SEBS block copolymers as novel materials to design transdermal patches. Int J Pharm. 2020;575:118975.
29. Li X, Luan S, Shi H, Yang H, Song L, Jin J, et al. Improved biocompatibility of poly (styrene-b-(ethylene-co-butylene)-b-styrene) elastomer by a surface graft polymerization of hyaluronic acid. Colloids Surf B Biointerfaces. 2013;102:210-7.
30. Srimaneepong V, Rokaya D, Thunyakitpisal P, Qin J, Saengkiettiyut K. Corrosion resistance of graphene oxide/silver coatings on Ni–Ti alloy and expression of IL-6 and IL-8 in human oral fibroblasts. Sci Rep. 2020;10(1):3247.
31. Yung TY, Lu WF, Tsai KC, Chen JS, Pang KN, Tzeng YC, et al. Corrosion resistance and thermal conductivity enhancement of reduced graphene oxide–BaSO4–epoxy composites. Polymers (Basel). 2022;14(15):3144.
32. Okazaki S, Ohhashi T, Nakao S, Hirose Y, Hitosugi T, Hasegawa T. Wet etching of amorphous TiO_2 thin films Using H_3PO_4–H_2O_2 aqueous solution. Jpn J Appl Phys. 2013;52(9R):098002. http://doi.org/10.7567/JJAP.52.098002.
33. ASTM International. F2516-18. Standard Test Method for Tension Testing of Nickel-Titanium Superelastic Materials. West Conshohocken: ASTM International; 2018
34. Yamauchi K, Ohkata I, Tsuchiya K, Miyazaki S. Shape memory and superelastic alloys: applications and technologies. Amsterdam: Elsevier; 2011.
35. Firstov GS, Vitchev RG, Kumar H, Blanpain B, Van Humbeeck J. Surface oxidation of NiTi shape memory alloy. Biomaterials. 2002;23(24):4863-71.
36. Wang MH, Li Q, Li X, Liu Y, Fan LZ. Effect of oxygen-containing functional groups in epoxy/reduced graphene oxide composite coatings on corrosion protection and antimicrobial properties. Appl Surf Sci. 2018;448:351-61.
37. Han Q, Wang R, Xue Y, Camilli L, Yu G, Luo B. Optimization strategies for graphene-based protection coatings: a review. Corros Rev. 2024;43(1):23-59.
38. Fernández-Sotillo A, Ferreira-Aparicio P. Durable corrosion-resistant coating based in graphene oxide for cost-effective fuel cells components. iScience. 2023;26(5):106569.
39. Xue B, Yu M, Liu J, Liu J, Li S, Xiong L. Corrosion protection of AA2024-T3 by sol-gel film modified with graphene oxide. J Alloys Compd. 2017;725:84-95.
40. Chauhan DS, Quraishi MA, Ansari KR, Saleh TA. Graphene and graphene oxide as new class of materials for corrosion control and protection: present status and future scenario. Prog Org Coat. 2020;147:105741.
41. Zhou C, Hong M, Yang Y, Hu N, Zhou Z, Zhang L, et al. Engineering sulfonated polyaniline molecules on reduced graphene oxide nanosheets for high-performance corrosion protective coatings. Appl Surf Sci. 2019;484:663-75.
42. Xavier JR, Vinodhini SP, Raja Beryl J. Anti-corrosion and flame-retardant properties of environmentally benign smart functionalized WS2/rGO in epoxy coatings for enhanced steel structural protection in natural seawater. Mater Today Commun. 2024;38:107842.
43. Zhang L, Duan Y, Gao Z, Ma J, Liu R, Liu S, et al. Graphene enhanced anti-corrosion and biocompatibility of NiTi alloy. NanoImpact. 2017;7:7-14.

Data Availability

Data will be made available on request.